Design and Validation of a Localisation and Control System for a Nonholonomic vehicle

JoÃčo Barbosa
joao.vitor.barbosa@ist.utl.pt

Instituto Superior Técnico, Lisboa, Portugal

Abstract

This paper proposes and experimentally validates a docking system for a differential drive robot, composed by a localisation system and full state feedback control law. Observation of the state consists of a single landmark-based mobile robot localization system, composed by two filters, one for attitude estimation and the other for position estimation. The estimation is carried out in the body-frame allowing for the model kinematics to be LPV (Linear Parameter Varying). The resultant globally stable estimators are parametrized by odometry data and updated by landmark position and attitude measurements provided by an on-board RGB-D (red, green, blue and depth) sensor. Experiments were carried out, making use of a wheeled mobile robot and a Qualysis Motion Tracking System for ground truth validation of the proposed methods. Attitude and position as well as linear and angular slippages, both proven observable, are estimated, resulting in an effective real-time localisation system without requiring the landmark to be always visible. A statistical study of the estimation error was carried out to verify the Gaussian noise assumptions inherent to the use of Kalman filtering. Error convergence is achieved regardless of the initial estimate of both position and attitude, validating the system global stability. The docking problem is solved by finding a smooth, time-invariant, globally asymptotically stable feedback control law using Lyapunov techniques by expressing the kinematics of the robot in polar coordinates, allowing for a very human-like closed-loop steering that drives the robot to a certain goal with a desired attitude and a tunable curvature. Simulations of the docking problem are presented to illustrate the performance of the system and it is also validated by performing tests on the aforementioned real robot.
Keywords: Docking, Localisation, Mobile Robots, Kalman Filter, Lyapunov

I. Introduction

Mobile robot tasks in industrial facilities most often include the transportation of cargo or raw/processed materials from one point to the other, being then essential for the robot to be able to identify packages, localise them in its referential so as to be able to approach and transport them. Although localisation algorithms for unstructured environments often show very good results, their precision may not be enough for tasks such as the docking of a mobile robot in a cargo pallet or a charging station.

Ever since mobile robots began to be used, the docking problem has been studied in a number of different approaches, given its important role in the automatism of a robots' task, since it is desirable that the robot is able to sustain long term activity by recharging itself [9]. The solutions found in the literature to solve this problem vary both in algorithm and sensor payload. One approach, defined as visual servoing, of which an early contribution was [2], is to represent a given task directly by an error relative to a goal image to be captured by the vision system. This approach saw a greater development from 1990 onward with works such as [7], [10], with a great contribute of the task function approach [16]. Visual servoing benefits from contributes with out-of-body cameras, i.e., Camera-Space Manipulation (CSM) [17], Mobile Camera-Space Manipulation (MCSM) which extends the latter with body embedded cameras and more recently [12] which computes the goal configuration using visual landmarks. Other approaches to the docking problem include the computation of feedback control laws by using Lyapunov and backstepping techniques that lean on Ultra-Short Baseline (USBL) acoustic positioning [4] applied on the underwater counterpart of this work, the use of electromagnetic homing systems [8], optical guidance approaches such as [15] and computing the deceleration needed by a robot, resorting to an estimation of a *time-to-contact* (τ) through optical flow field divergence measurements of an image stream as in [14] and references therein. In [11] a method based on the direction of arrival (DOA) of signals transmitted by RFID transponders is proposed, showing that a robot can dock in a station transmitting through an RFID by using two antennae installed on-board of the vehicle. A localisation method using homography between several consecutive images is proposed in [6]. A method proposing the estimation of the position and orientation of a visual landmark is proposed in [13] for later docking and automatic recharging, thus being similar to the work here presented.

This work proposes an innovative method of localisation of a landmark in the body frame of a robot based on Linear Kalman Filters by using feature recognition with an RGB-D camera and odometry readings from optical wheel encoders. Furthermore, the filtering solution is also meant to be able to estimate both linear and angular slippages by making use of the ability to recognise both position and attitude of a given landmark in the body frame of the robot. The second objective of this work is the design of a control feedback law that drives the robot from an initial position to a desired location with a given angle of arrival, commonly known as docking or parking problem. Having the robot be guided by a vision system allows for more versatility in an industrial facility regarding docking stations, positioning of cargo pallets, consequently simplifying the overall task map building and task planning, dropping the need of extreme precision regarding these actions.

The present paper is organised as follows: Section II presents the architecture of the proposed localisation system, followed by Section III where a brief description of the reference frames and their relations is carried out. The description of the kinematics and filtering solutions for both

attitude and position are respectively carried out in Section IV and Section V. Details on the feedback control law used in this work are presented in Section VI, which is followed by the results of real-time experiments in Section VII. Finally, some conclusions on the overall performance of the proposed strategies are drawn in Section VIII.

II. Localisation System Architecture

The proposed landmark-based on-board localization system, depicted in Fig. 1, is composed by three modules: i) the landmark detector module that consists of the algorithm that will process the RGB and depth images in order to obtain measurements of the landmark position and orientation in the robot frame; ii) a sub-optimal position estimator based on a Kalman Filter; iii) an optimal attitude estimator, also based on Kalman Filter. These modules rely, as stated before, on the sensor package composed by a RGB-D camera, that will provide the landmark detector with the images, and both optical encoders attached to the wheels that provide angular and linear velocity readings. The velocity readings are, however, not derived from the encoder readings directly, but from the commands stored in the controller. The attitude and position are respectively described in Section IV and Section V.

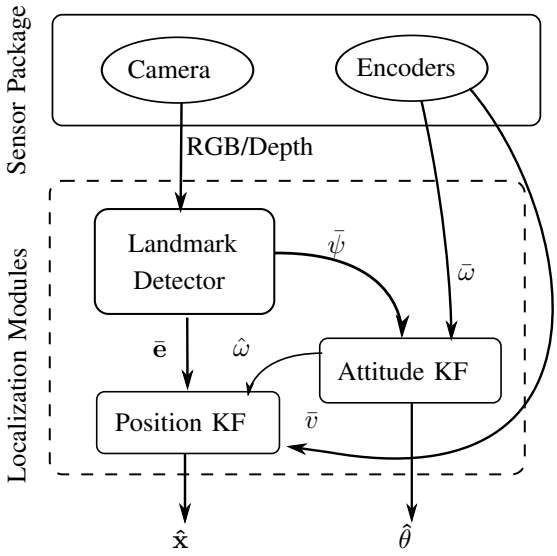

Fig. 1: Estimator Modules

III. Model Description

The mobile robot scenario of operation under study in this work is depicted in Fig. 2, where the frame $\{I\}$ is fixed to Earth, which is considered to be stationary for the purposes of this study, thus making it an inertial frame. Frame $\{B\}$ can be defined as being attached to the vehicle and is hence designated by body-fixed frame. Both frames $\{I\}$ and $\{B\}$ are defined, respectively, by the orthonormal basis $\{{}^I\mathbf{i}_I, {}^I\mathbf{j}_I\} \in \mathbb{R}^2$ and $\{{}^I\mathbf{i}_B, {}^I\mathbf{j}_B\} \in \mathbb{R}^2$.

In order to transform a position written in $\{B\}$ into one written in $\{I\}$, a transformation needs to be executed. The translation is defined by the body-fixed frame position in

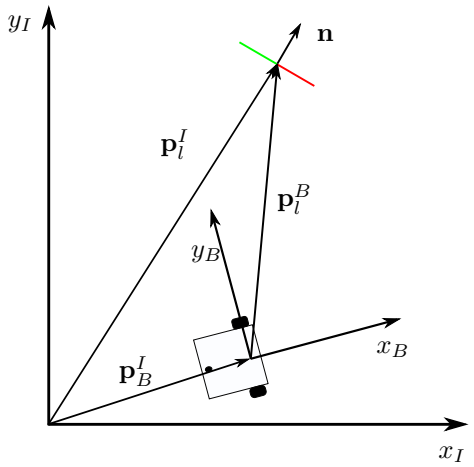

Fig. 2: Reference frames.

the inertial frame $\mathbf{p}_B^I$, and so the landmark position in both frames follows (1).

$$\mathbf{p}_B^I(t) + {}^I\mathbf{p}_l^B(t) = \mathbf{p}_l^I(t), \tag{1}$$

where ${}^I\mathbf{p}_l^B(t) \in \mathbb{R}^2$ is the landmark position in $\{B\}$ expressed in $\{I\}$ and $\mathbf{p}_l^I(t)$ is the landmark position in $\{I\}$, expressed in the latter. The landmark position in the body fixed frame $\mathbf{p}_l^B(t) \in \mathbb{R}^2$ needs to be derived and will henceforth, for a matter of simplicity, be denoted as $\mathbf{e}(t)$.

The rotation matrix from $\{B\}$ to $\{I\}$ that simplifies (1) is denoted by ${}^I\mathbf{R}_B(t) \in SO(2)$. A matrix that belongs to the special orthogonal rotation matrices group preserves the inner product of two transformed vectors, thus preserving their length and relative orientation. This rotation matrix respects the following properties.

- It has a unitary determinant: $\det\left({}^I\mathbf{R}_B(t)\right) = 1$,
- It creates a correspondence between representations in $\{B\}$ and $\{I\}$,${}^I\mathbf{e}(t) = {}^I\mathbf{R}_B(t){}^B\mathbf{e}(t)$,
- The inverse of this rotation is its transpose, ${}^I\mathbf{R}_B(t)^{-1} = {}^I\mathbf{R}_B(t)^T$ and, by definition, it transforms vectors from $\{I\}$ to $\{B\}$:$\mathbf{e}(t) = {}^I\mathbf{R}_B(t)^T{}^I\mathbf{e}(t)$
- The rotation kinematics is given by (3).

$$ {}^I\dot{\mathbf{R}}_B(t) = \mathbf{S}(\omega)\mathbf{R}(t) \tag{2}$$

where

$$\mathbf{S}(\omega) = \begin{bmatrix} 0 & -\omega \\ \omega & 0 \end{bmatrix},$$

and $\omega \in \mathbb{R}$ is the angular velocity of the body-fixed frame. The rotation ${}^I\mathbf{R}_B(t)$ will henceforth be denoted as $\mathbf{R}(t)$ for simplicity of notation. It is straightforward to show that the inverse rotation follows a similar expression to (3) by taking the derivative on both sides of $\mathbf{R}^T\mathbf{R} = \mathbf{I}$ and making the necessary substitutions

$$\dot{\mathbf{R}}^T(t) = -\mathbf{S}(\omega)\mathbf{R}^T(t). \tag{3}$$

IV. Optimal Attitude and Angular Slippage Estimation

This section will focus on deriving the attitude estimator. Firstly the kinematic model will be described, giving then place for a brief observability analysis and then defining the estimator. The proposed kinematic system estimates explicitly the unavoidable angular slippage that may occur due to the lack of knowledge of the contact points with the floor as

well as the lack of precision in the measurement of each wheel radius or asymmetries in mechanical construction. Here the angular slippage $s(t)$ is considered to be slow time-varying or even constant ($\dot{s} = 0$). The model that describes the attitude system is given by the kinematics and the output equations

$$\dot{\theta}(t) = \mathbf{A}^{\theta}\theta(t) + \mathbf{B}^{\theta}\omega(t) + \nu(t), \tag{4}$$

and

$$y(t) = \mathbf{C}^{\theta}\theta(t) + \eta(t), \tag{5}$$

respectively, where

$$\theta(t) = \begin{bmatrix} \psi(t) \\ s(t) \end{bmatrix},$$
$$\mathbf{A}^{\theta} = \begin{bmatrix} 0 & -1 \\ 0 & 0 \end{bmatrix},$$
$$\mathbf{B}^{\theta} = \begin{bmatrix} -1 \\ 0 \end{bmatrix},$$
$$\mathbf{C}^{\theta} = \begin{bmatrix} 1 & 0 \end{bmatrix}.$$

and $\nu(t)$ and $\eta(t)$ are the plant noise and output noise, respectively, both assumed to respect an unbounded normal distribution, i.e,

$$\nu(t) \sim N(\mathbf{0}, \mathbf{Q}_{\theta})$$
$$\eta(t) \sim N(\mathbf{0}, \mathbf{R}_{\theta}).$$

This model addresses the landmark as if it is moving in the body reference system and so $\psi(t)$ represents the landmark attitude in it, which as stated before, is under the assumption that it is possible to define a unique reference system in the said landmark, and that the camera is able to detect its orientation. Assuming a constant angular velocity between two sampling instants, the state transition equation for this linear time invariant system is

$$\theta(k+1) = \mathbf{\Phi}^{\theta}(T)\theta_k + \mathbf{G}_k^{\theta}\omega_k + \nu_k, \tag{6}$$

in which ω_k is the measured angular velocity obtained using the command sent to the dual-motor driver, $\mathbf{\Phi}^{\theta}(T) = \exp(A^{\theta}T_k)$, $\mathbf{G}_k^{\theta} = \omega_k \int_0^{T_k} \mathbf{\Phi}^{\theta}(T_k - \tau)\left(\mathbf{B}^{\theta}\right) d\tau$ and T_k is the time between samples k and $k+1$, a measured quantity, rather than a constant sampling period.

The state vector needs to be estimated by using the output equation, which in turn does not, apparently, give information about all the states, and so a simple observability analysis is carried out next. Since the continuous system is LTI, (7) is sufficient to assess the observability of the system

$$\mathcal{O}_a = \begin{bmatrix} \mathbf{C} \\ \mathbf{CA} \end{bmatrix} = \begin{bmatrix} 1 & 0 \\ 0 & -1 \end{bmatrix} \tag{7}$$

The observability matrix verifies $rank(\mathcal{O}_a) = 2$, which renders the attitude state vector observable.

The attitude kinematics and output system are completely defined and so it is now possible to define the dynamics of the state vector estimate, making use of the celebrated Kalman filter,

$$\hat{\theta}_k = \mathbf{\Phi}^{\theta}(T)\hat{\theta}_{k-1} + \mathbf{G}^{\theta}(T)\omega_k + \mathbf{K}_k^{\theta}\left[\bar{\psi}_k - \hat{\psi}_k\right], \tag{8}$$

where $\mathbf{K}_k^{\theta}$ is the Kalman gain computed for the attitude system in time kT. The Kalman gain is dynamically computed at each iteration, i.e., every time a landmark is detected by the camera algorithm, by using (9)

$$\mathbf{K}_k^{\theta} = \mathbf{P}_k^{\theta}\mathbf{C}^{\theta T}\left[\mathbf{C}^{\theta}\mathbf{P}_k^{\theta}\mathbf{C}^{\theta T}\right]^{-1}, \tag{9}$$

where $\mathbf{P}^{\theta}{}_k = E\left[\tilde{\theta}\,\tilde{\theta}^T\right]$ is the estimation error covariance matrix and $\tilde{\theta}$ is the estimation error. This matrix is also dynamically computed by (10) whenever information from the wheels is available and (11) when the landmark is detected by the image processing module

$$\mathbf{P}_{k|k-1}^{\theta} = \mathbf{\Phi}_k^{\theta}\mathbf{P}_{k-1|k-1}^{\theta}\mathbf{\Phi}_k^{\theta T} + \mathbf{Q}_k^{\theta}, \tag{10}$$

$$\mathbf{P}_{k|k}^{\theta} = (\mathbf{I} - \mathbf{K}_k^{\theta}\mathbf{C}_k^{\theta})\mathbf{P}_{k|k-1}^{\theta}(\mathbf{I} - \mathbf{K}_k^{\theta}\mathbf{C}_k^{\theta T}) + \mathbf{K}_k^{\theta}\mathbf{R}_k^{\theta}\mathbf{K}_k^{\theta T}. \tag{11}$$

V. Sub-Optimal Position and Linear Slippage Estimation

In order to have a localization system working in $\{B\}$, as stated above, we need to be able to express $\dot{\mathbf{e}}(t)$ for the position of the landmark kinematic derivation. After having completely defined the model of the robot environment in Section III, we start by expressing the robot's position in $\{I\}$ kinematics in (12)

$$\dot{\mathbf{p}}(t) = {}^{I}\mathbf{R}_B(t)\mathbf{u}(t), \tag{12}$$

where $\mathbf{u}(t) = [v(t)\ \ 0]$ and $v(t) \in \mathbb{R}$ is the robot velocity in the body-fixed frame. By expressing the product of (1) by $\mathbf{R}^T$ we get the position $\mathbf{e}(t)$ expressed in order of $\mathbf{p}_l$ and $\mathbf{p}$ each corresponding to the landmark position and $\{B\}$ position in $\{I\}$ (respectively $\mathbf{p}_l^I$ and $\mathbf{p}_B^I$).

$$\mathbf{e}(t) = \mathbf{R}(t)^T(\mathbf{p}_l(t) - \mathbf{p}(t)), \tag{13}$$

which, once the time derivative is taken gives

$$\dot{\mathbf{e}} = \dot{\mathbf{R}}^T(t)(\mathbf{p_l}(t) - \mathbf{p}(t)) + \mathbf{R}^T(t)\left(\dot{\mathbf{p}}_l(t) - \dot{\mathbf{p}}(t)\right). \tag{14}$$

Considering that the landmark will be static in the inertial reference system, the term where $\dot{\mathbf{p}}_l(t)$ will be dropped, and by using (13) and (12) in (14) we get

$$\dot{\mathbf{e}} = -\mathbf{S}(\omega)\mathbf{R}^T(t)(\mathbf{p}_l(t) - \mathbf{p}(t)) - \mathbf{R}^T(t)\dot{\mathbf{p}}(t), \tag{15}$$

and if we further use the substitutions of (13) and (12) we will get the simplified equation in (16)

$$\dot{\mathbf{e}}(t) = -\mathbf{S}(\omega)\mathbf{e}(t) - \mathbf{u}(t). \tag{16}$$

It can be further assumed that the common mode velocity $v(t)$ can suffer from a biased measurement due to slippage. The velocity could then be expressed as $v(t) = \bar{v}(t) + b$ where b is the constant or slow varying bias and $\bar{v}(t)$ is the measured linear velocity, while $v(t)$ is the true linear velocity. If the state vector is $\mathbf{x}(t) = [\mathbf{e}^T(t)\, b(t)]^T$ then the matrix expression for the kinematics of the position will be given by (17)

$$\begin{aligned}\dot{\mathbf{x}}(t) =& \mathbf{A}(\omega(t))\mathbf{x}(t) + \mathbf{B}\bar{v}(t) + \mathbf{v}(t) \\ =& \begin{bmatrix} 0 & \omega & -1 \\ -\omega & 0 & 0 \\ 0 & 0 & 0 \end{bmatrix}\mathbf{x}(t) + \begin{bmatrix} -1 \\ 0 \\ 0 \end{bmatrix}\bar{v}(t) + \mathbf{v}(t),\end{aligned} \tag{17}$$

where $\mathbf{v}(t) \in \mathbb{R}^3$ is the white plant noise caused by the model uncertainty and follows the following properties

$$E[\mathbf{v}(t)] = 0, \quad \forall t \in \mathbb{R} \tag{18}$$

$$E[\mathbf{v}(t)\mathbf{v}^T(\tau)] = \mathbf{Q}\delta(t - \tau). \tag{19}$$

The output equation of the system can be expressed by (20) since the camera sensor gives the landmark localization in $\{B\}$

$$\begin{aligned}\mathbf{y}(t) &= \begin{bmatrix} 1 & 0 & 0 \\ 0 & 1 & 0 \end{bmatrix} \mathbf{x}(t) + \mathbf{w}(t) \\ &= \mathbf{C}\mathbf{x}(t) + \mathbf{w}(t) = \mathbf{e}(t) + \mathbf{w}(t), \end{aligned} \tag{20}$$

where $\mathbf{w}(t)$ represents the noise generated by the camera sensor as well as the detection algorithm and has similar properties to those of the plant noise

$$E[\mathbf{w}(t)] = 0, \quad \forall t \in \mathbb{R} \tag{21}$$

$$E[\mathbf{w}(t)\mathbf{w}^T(\tau)] = \mathbf{R}\delta(t-\tau), \quad \forall t, \tau \in \mathbb{R}. \tag{22}$$

Also, both the plant and the sensor noise are uncorrelated, which can be expressed as

$$E[\mathbf{w}(\eta)\mathbf{v}(\tau)] = 0, \quad \forall \eta, \tau \in \mathbb{R}. \tag{23}$$

By taking an identical approach to the one in Section IV, the LPV discrete system is defined as

$$\mathbf{x}_k = \mathbf{\Phi}(\omega_k)\mathbf{x}_{k-1} + \mathbf{G}_k v_{k-1} + \mathbf{v}_k, \tag{24}$$

where the transition matrix $\mathbf{\Phi}_k$ is expressed by (25)

$$\begin{aligned}\mathbf{\Phi}_k &= \exp\left(\int_0^{T_k} \mathbf{A}(\tau)d\tau\right) \\ &= \begin{bmatrix} c(\omega_k T_k) & s(\omega_k T_k) & -\frac{s(\omega_k T_k)}{\omega_k} \\ -s(\omega_k T_k) & c(\omega_k T_k) & \frac{1-c(\omega_k T_k)}{\omega_k} \\ 0 & 0 & 1 \end{bmatrix}, \end{aligned} \tag{25}$$

$\mathbf{v}_k$ is the discrete white noise and $\mathbf{G}_k$ is the discrete input matrix expressed in (26)

$$\mathbf{G}_k = \int_{t_{k-1}}^{t_k} \mathbf{\Phi}(\tau, t_{k-1})\mathbf{B}d\tau = \begin{bmatrix} -\frac{\sin\omega_{k-1}T}{\omega_{k-1}} \\ \frac{1-\cos\omega_{k-1}T}{\omega_{k-1}} \\ 0 \end{bmatrix}. \tag{26}$$

In order for the entire state vector $\mathbf{x}$ yo be estimated, the system needs to be observable, since the observation matrix $\mathbf{C}$ does not give information about the slippage directly. In the position model case, since the kinematics are LTV, this is assured if and only if the observability gramian $\mathbf{W_O}(t_1, t_0)$ defined by (27) is non-singular. It takes the form

$$\begin{aligned}\mathbf{W_O}(t_1, t_0) &= \int_{t_0}^{t_1} \Phi^T(\tau, t_0) C^T C \Phi(\tau, t_0) d\tau \\ &= \int_{t_0}^{t_1} \begin{bmatrix} 1 & 0 & a \\ 0 & 1 & b \\ a & b & c \end{bmatrix} d\tau, \end{aligned} \tag{27}$$

where

$$\begin{aligned} a &= -\frac{(\tau - t_0)\sin(\theta - \theta_0)}{\theta - \theta_0}, \\ b &= \frac{(\tau - t_0)(\cos(\theta - \theta_0) - 1)}{\theta - \theta_0}, \\ c &= 2\left(\frac{\tau - t_0}{\theta - \theta_0}\right)^2 (1 - \cos(\theta - \theta_0)), \end{aligned}$$

which can be particularized for the linear movement case ($\omega = 0$), resulting in

$$\mathbf{W_O}(t_1, t_0)|_{\omega=0} = \begin{bmatrix} \Delta t & 0 & -\Delta t \\ 0 & \Delta t & 0 \\ -\Delta t & 0 & -\Delta t^2 \end{bmatrix}$$

The integral does not change the matrix rank and so $rank(W_O) = 3$ which is the same as the number of states present in the state vector, thus rendering this system observable.

The position estimator will perform a sub-optimal estimation since the angular velocity that parametrizes the state transition matrix of this system is meant to take into account the angular slippage whose estimation is described in Section IV. Nevertheless, the equation that describes the estimate dynamics is similar to the one used for the attitude system estimate and is expressed by (28)

$$\hat{\mathbf{x}}_k = \mathbf{\Phi}^{\mathbf{x}}(\hat{\omega}_k, T)\hat{\mathbf{x}}_{k-1} + \mathbf{B}^{\mathbf{x}} v_k + \mathbf{K}_k^{\mathbf{x}}\left[\bar{\mathbf{e}}_k - \hat{\mathbf{e}}_k\right]. \tag{28}$$

The Kalman gain for this estimator is calculated in the exact same way as in the attitude estimator, using (9), only using the appropriate matrices $\mathbf{R}^{\mathbf{x}}$, $\mathbf{C}^{\mathbf{x}}$, $\mathbf{P}^{\mathbf{x}}$ and $\mathbf{Q}^{\mathbf{x}}$.

VI. Docking problem

Let the state vector to be controlled be $\mathbf{z} = [e_x\ e_y\ \psi]^T$, from (4) and (17) we get that its kinematics can be expressed as

$$\dot{\mathbf{z}} = \mathbf{f}_\omega(\mathbf{z})\omega + \mathbf{f}_v(\mathbf{z})v, \tag{29}$$

where

$$\mathbf{f}_\omega = \begin{bmatrix} e_y \\ -e_x \\ -1 \end{bmatrix}, \quad \mathbf{f}_v = \begin{bmatrix} -1 \\ 0 \\ 0 \end{bmatrix}.$$

The present work follows Lyapunov's direct method of finding a scalar energy-like function $V(\mathbf{z})$ and devise a control law $\mathbf{u}(\mathbf{z})$ that ensures the resulting closed-loop system is asymptotically stable (the goal is to park the vehicle in a position $\mathbf{z}^*$). This leads to a smooth and time invariant control law. However, a theorem developed by Brockett shown in [5], states that, for systems in the structure

$$\dot{\mathbf{z}} = \sum_{i=1}^{m} \mathbf{f}_i(\mathbf{z})u_i,$$

with vectors $\mathbf{f}_i(\mathbf{z})$ being linearly independent and continuously differentiable at a point z^*, then there exists a stabilization solution, with a smooth and time invariant feedback law, if and only if $m = n$, where n is the order of the system, meaning there need to be the same number of control parameters as the dimension of the state vector to be controlled. The system in (29) does not respect the last condition and clearly has $\mathbf{f}_\omega$ and $\mathbf{f}_v$ independent at the origin. This would then require the use of time-varying or discontinuous control laws in order to achieve the desired stabilization. Seeing as the need of stabilizing n states at a point $\mathbf{z}^*$ is still the objective, then only a system with singularities is of interest. With this in mind, a new system is proposed in [3]. The said system represented in (30) is based on a state vector that is isomorphic with the one in (29), characterized by the isomorphism $g : \mathbb{R}^3 \setminus \{\mathbf{0}\} \mapsto \mathbb{R}^3 \setminus \{\mathbf{0}\}$

$$\begin{cases} e = \sqrt{e_x^2 + e_y^2} \\ \alpha = atan(e_y/e_x) \\ \phi = atan(e_y/e_x) - \psi \end{cases},$$

leading to the kinematics

$$\begin{cases} \dot{e} = -v\cos\alpha \\ \dot{\alpha} = -\omega + v\frac{\sin\alpha}{e} \\ \dot{\phi} = v\frac{\sin\alpha}{e} \end{cases}. \tag{30}$$

The new state vector is depicted in Figure 3. Due to

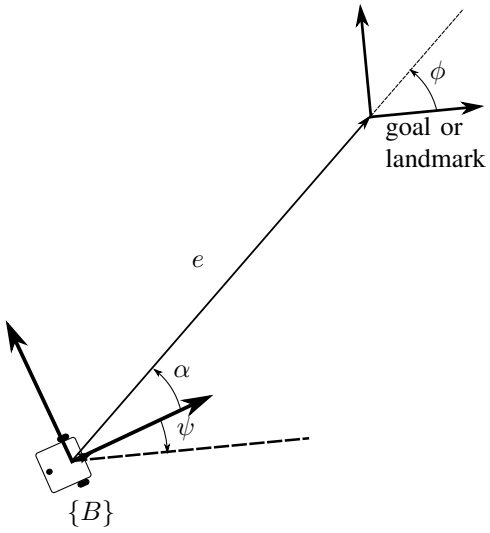

Fig. 3: Depiction of new state vector.

the singularity at the origin, Brockett's theorem no longer applies, since the regularity assumptions do not hold, and so the asymptotic stabilization of (30) is possible. One then cannot formally use the definition of equilibrium point to describe the origin, since it is now located in the frontier of the open set of validity of the system dynamics. The objective of the control law is then to asymptotically drive the system to $\mathbf{z_p}^* = [0 \quad 0 \quad 0]^T$ without attaining $e = 0$ in a finite time, where $\mathbf{z_p} = [e \quad \alpha \quad \phi]$ is henceforth the notation used for the new state vector. A simple choice for a candidate Lyapunov function is the often used quadratic error form

$$V(\mathbf{z}) = \underbrace{\frac{1}{2}\lambda e^2}_{V_1} + \underbrace{\frac{1}{2}\alpha^2 + \frac{1}{2}h\phi^2}_{V_2}, \quad \lambda, h > 0 \tag{31}$$

where λ and h are positive weighting constants that will later on help shape the control law. By separating the scalar function in two terms, we have that the first term refers to the error in distance to the target position, and the second term corresponds to the to a "alignment vector" error $[\alpha \quad h\phi]$. It is clear by now that the a candidate of a scalar function has been chosen and then a function $\mathbf{u}(\mathbf{z_p})$ will be derived in order for the behaviour of V along the trajectory of (30) to drive the state asymptotically to the origin. Taking then the derivative $\dot{V}$, given by

$$\begin{aligned} \dot{V} &= \lambda e\dot{e} + \left(\alpha\dot{\alpha} + h\phi\dot{\phi}\right) \\ &= \lambda e v\cos\alpha + \alpha\left[-\omega + v\frac{\sin\alpha(\alpha + h\phi)}{\alpha e}\right]. \end{aligned} \tag{32}$$

The first term of (32) can be made non-positive by letting

$$v = \gamma e\cos\alpha, \quad \gamma > 0, \tag{33}$$

leading to

$$\dot{V}_1 = -\lambda\gamma\cos^2\alpha e^2 \leq 0. \tag{34}$$

This choice of linear velocity control law ensures that the validity of (30) throughout the parking problem, since V_1 is lower bounded and non-increasing, making it asymptotically converge to a non negative finite limit, thus ensuring e exhibits the same behaviour. The same strategy is applied to the second term, and so expression for the angular velocity control law is

$$\begin{aligned} \omega &= k\alpha + v\frac{\sin\alpha(\alpha + h\phi)}{\alpha e} \\ &\overset{(33)}{=} k\alpha + \gamma\frac{\cos\alpha\sin\alpha(\alpha + h\phi)}{\alpha}. \end{aligned} \tag{35}$$

The derivative of the total Lyapunov function then becomes

$$\dot{V} = -\gamma\left(\cos^2\alpha\right)e^2 - k\alpha^2 \leq 0, \tag{36}$$

which is negative semi definite. A fundamental result of calculus lets us establish that, given the non increasing nature of V and given that its lower boundedness by zero, then it converges to a non negative limit. This in turn, together with the radial unboundedness of V, assures the boundedness of the state trajectories for any bounded initial conditions. By then using LaSalle's Theorem, and noting that $E = \{\mathbf{z_p} \in \mathbb{R}^3 : \dot{V}(\mathbf{z_p}) = 0\}$, inspection of (36) indicates that the state trajectory will converge to the largest invariant set M characterized by a state of the form $[0 \quad 0 \quad \phi]$. To prove that the origin is the only solution that can identically stay in E, the closed-loop kinematics system must be inspected

$$\begin{cases} \dot{e} = \gamma e\cos^2\alpha \\ \dot{\alpha} = -k\alpha - \gamma h\frac{\cos\alpha\sin\alpha}{\alpha}\phi \\ \dot{\phi} = \gamma\cos\alpha\sin\alpha \end{cases} \qquad e > 0. \tag{37}$$

Given the convergence of e and α to zero, then both time derivates $\dot{e}$ and $\dot{\phi}$ converge to zero. The convergence of $\dot{\phi}$ allied with the boundedness of the trajectory asserts that ϕ must converge to a finite limit $\bar{\phi}$ over time. It then follows that $\dot{\alpha}$ tends to the limit $-\gamma h\bar{\phi}$. Given the bounded nature of the trajectory, the uniform continuity of $\dot{\alpha}$ follows, allowing for the use of Barbalat's Lemma which results in $\dot{\alpha}$ converging to zero, which in turn confirms that $\bar{\phi} = 0$. This then proves that the largest invariant set M in E is

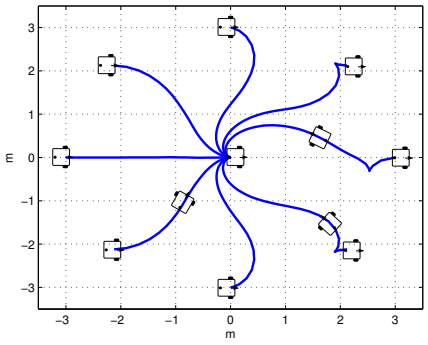

Fig. 4: Trajectories performed with $e(0) = 3$ and $\psi(0) = 0$

the origin, thus making the origin globally asymptotically stable. Note that the objective is to have the vehicle dock in a certain station with positive linear velocity, but it is possible

to obtain different trajectories by simply changing the goal objective (to for instance $\mathbf{z_p}^* = [0, \pm\pi, \pm\pi]$). A depiction of the trajectories performed by the system are depicted in Fig. 4, where a simulation was performed with $\gamma = 3$, $h = 1$ and $k = 6$.

As intended, the vehicle always arrives at the target location facing, which goes accordingly with state vector converging to the origin.

VII. Experimental Results

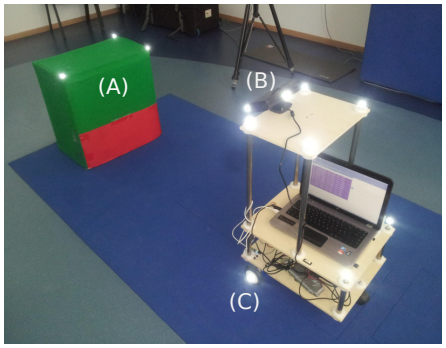

Fig. 5: Biomechanics Laboratory of Lisbon (Landmark (A), Robot prototype (B), Kinect Camera (C)).

Given the estimators and control law proposed in this work, they must be validated with experimental results. The focus of this section is the description of the experimental setup and the analysis of the estimation errors, as well as the validation of the docking solution. The ground truth validation data acquisition system used consists of a Qualisys™ Motion Tracking [1] system that uses 14 different cameras to track the position of reflectors placed upon the mobile robot. The characteristics of the tracking system are listed in Table I.

Cameras	14 Qualisys Pro Reflex 1000
Frequency	100 Hz
Markers	19 mm diam. passive retroreflectors
Precision	<1mm after calibration

TABLE I: Qualysis Motion Tracking system characteristics.

The robot prototype and landmark setup are shown in Fig. 5. Several passive retroreflectors, which are highlighted by the camera flash, were placed on the robot and landmark to provide redundant ground truth data. Below is a summary of the parameters and initialization of both Kalman Filters.

- Camera noise covariance: $\mathbf{R^x} = 1 \times 10^{-2}\mathbf{I}_2$ and $\mathbf{R}^\theta = 1 \times 10^{-2}$
- Plant noise covariance: $\mathbf{Q^x} = diag(4.1 \times 10^{-6}\mathbf{I}_2, 1 \times 10^{-8})$ and $\mathbf{Q}^\theta = diag(2 \times 10^{-5}, 1 \times 10^{-8})$
- Initial covariance matrix: $\mathbf{P}_0^{\mathbf{x}} = 1\mathbf{I}_3$ and $\mathbf{P}_0^\theta = 0.1\mathbf{I}_3$
- Initial conditions: $\hat{\mathbf{e}}$ and $\hat{\theta}$ were set to the real initial position, and both bias estimates $\hat{b}$ and $\hat{s}$ were set to zero.

It is also important to bear in mind the position of the camera frame $\{C\}$ relative to the body-fixed frame $\{B\}$, defined by a translation and a rotation particularized below

$$\mathbf{p}_C^B = [0.090 \quad 0.03 \quad 0.775]^T\,(m),$$
$${}^B\mathbf{R}_C = \begin{bmatrix} c(\theta) & -s(\theta) & 0 \\ s(\theta) & c(\theta) & 0 \\ 0 & 0 & 1 \end{bmatrix},$$

where $\theta = 0.216\,(rad)$.

A. Localisation System Validation

This section comprises the localization results for two separate trajectories performed in a laboratory equipped with with a Qualisys motion tracking system. For an easier visualisation, only a portion of the first trajectory tested is depicted in Fig. 6, where *Estimate* refers to a correct initialization and *Estimate 2* to a wrong one, for global stability validation. The comparison between ground truth

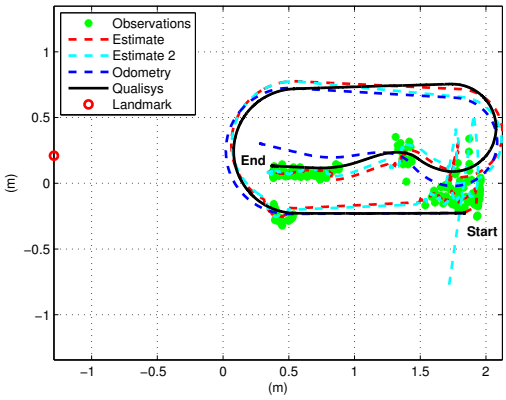

Fig. 6: Ground truth and Estimate.

data expressed in $\{B\}$ and the estimate is depicted in Figures 7 to 9. In these results neither of the slippages were being estimated, so the open-loop is carried-out with odometry data alone. The landmark is not always visible from the robot. The maximum difference between the estimated trajectory occurs after an unavailability of landmarks during a period of 30 seconds and also due to sensor faulty measurements at the end of the experiment. A statistical representation of these differences can be seen in Fig. 10.

When the same trajectory data is processed while also estimating the slippages, some improvement can be noticed, especially in the portion of the trajectory where both angular and linear velocities are maintained. The mentioned data set goes from 20 seconds to 50 seconds from the beginning of the experiment and the slippage estimation effect can be seen when comparing between Figures 7 to 9 with Figures 11 to 13. Since the robot kept both velocities nearly constant, the slippage estimation that took place until the 20 second mark was suitable until the 50 second mark, allowing for a reduced open-loop estimation error. The slippage estimations are depicted in Figures 14 and 15, where the shaded areas correspond to the time periods of landmark unavailability.

With the same data, a different test was conducted, this time forcing $b = -0.01\,(m/s)$. The slippage estimate behaviour is depicted in Fig. 16.

A more intuitive demonstration of the slippage estimation effect in the path estimation is depicted in Fig. 17 which

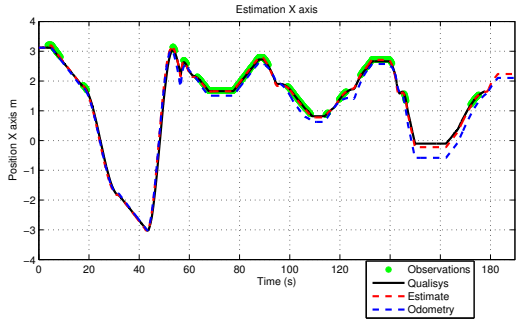

(a) Trajectory.

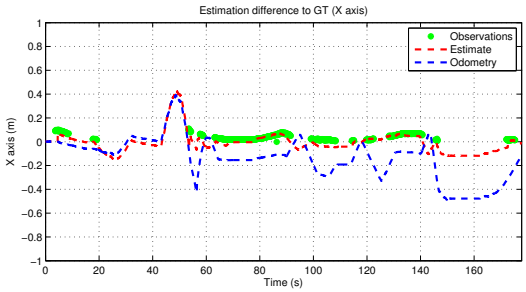

(b) Estimation error, relative to ground truth information.

Fig. 7: Estimate and ground truth in X axis.

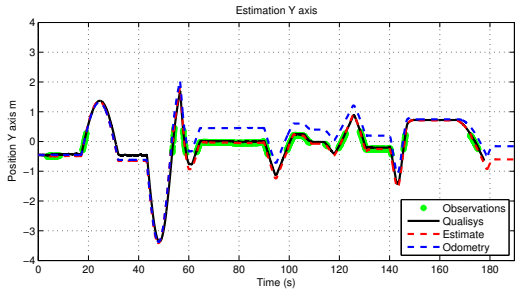

(a) Trajectory.

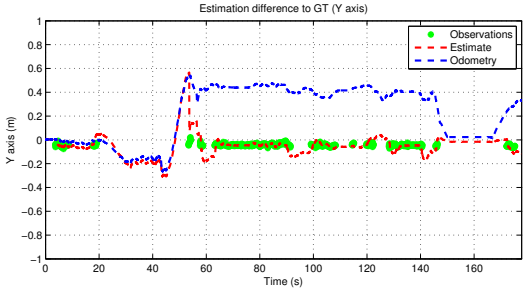

(b) Estimation error, relative to ground truth information.

Fig. 8: Estimate and ground truth in Y axis.

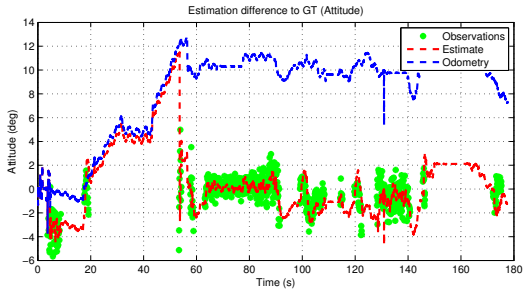

Fig. 9: Attitude estimate error, relative to ground truth information.

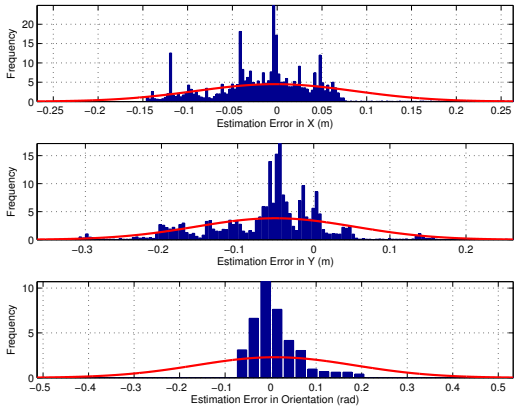

Fig. 10: Statistical study of estimation error relative to ground truth.

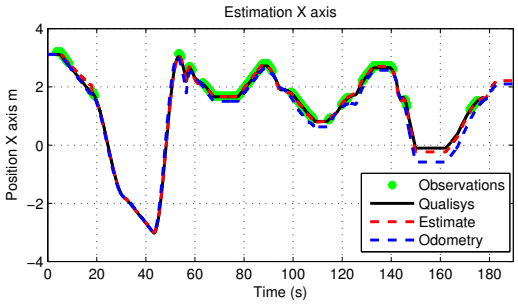

(a) Trajectory.

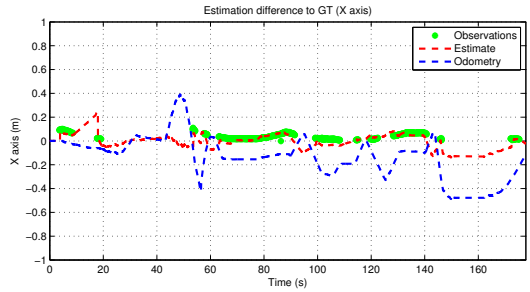

(b) Estimate error, relative to ground truth information.

Fig. 11: Estimate and ground truth in X axis.

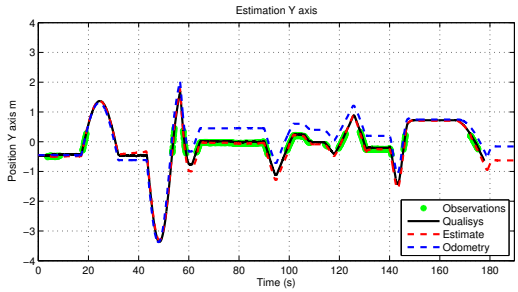

(a) Trajectory.

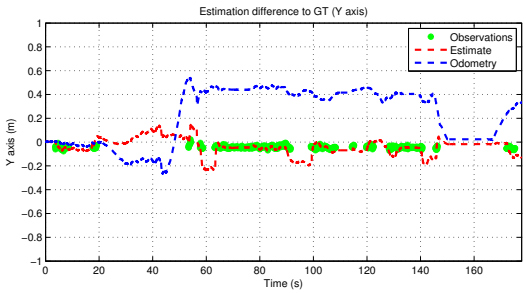

(b) Estimate error, relative to ground truth information.

Fig. 12: Estimate and ground truth in Y axis.

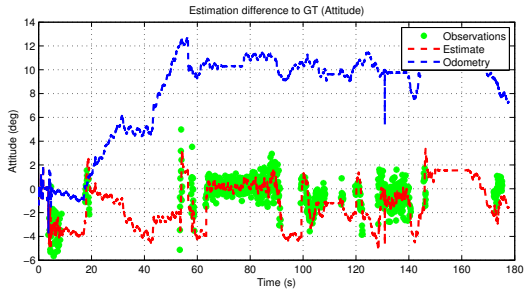

Fig. 13: Attitude Estimate error, relative to ground truth information.

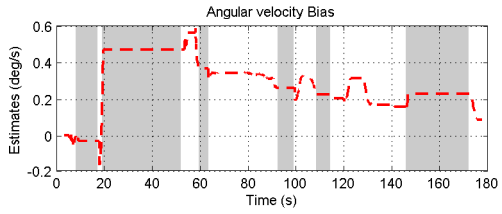

Fig. 14: Angular slippage estimation.

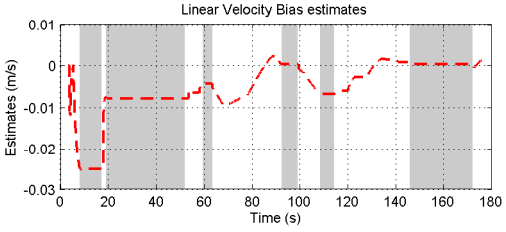

Fig. 15: Linear slippage estimation.

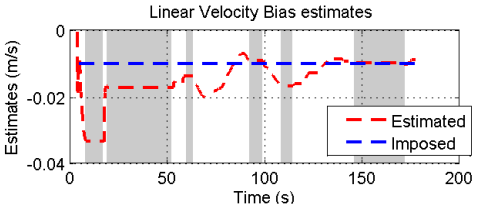

Fig. 16: Linear slippage estimation.

shows the data relative to a second simpler trajectory, where the robot maintained its linear velocity throughout the whole experiment, *Estimate* refers to an experiment without slippage estimation and *Estimate 2* is influenced by the slippage estimate.

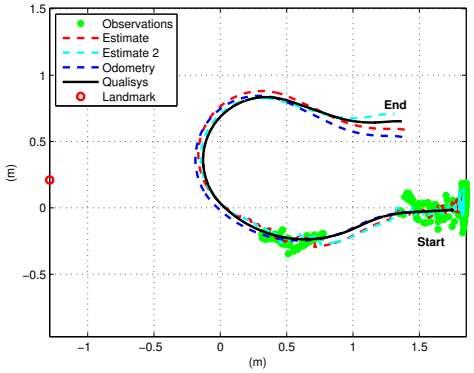

Fig. 17: Trajectory uninfluenced by slippage estimation.

B. *Docking System Validation*

In this section some tests regarding the full docking system are presented. The localisation system uses the same parameters as in previous sections, the landmark is considered to be the origin of the inertial frame and the goal of every experiment presented in this section was set $0.5\,m$ in front of the real landmark object being used. Also, in every experiment, unless stated otherwise, the initial estimate of the position was very near the real position of the mobile robot, seeing as the estimation filters were active before the feedback loop was enabled. In the first experiment saturations of $\omega_{max} = 0.2$ and $v_{max} = 0.2$ were applied.

It is possible to notice that the estimate shows no curvature at the end of the docking process, which goes towards the simulations before performed. Also, in Fig. 19 one can observe the effect that the correction of the estimate has in the command.

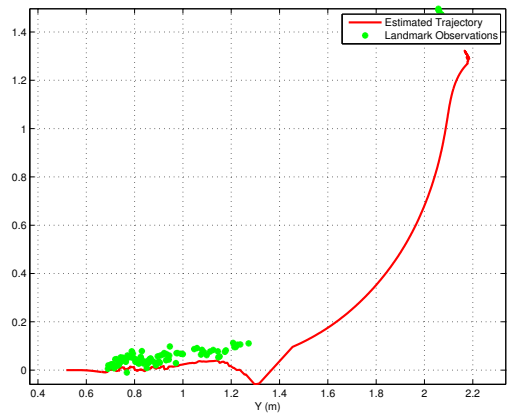

(a) Estimated trajectory.

(b) Initial position.

(c) Final position.

Fig. 18: Docking with $h = 20$, $k = 1$, $\gamma = 0.125$.

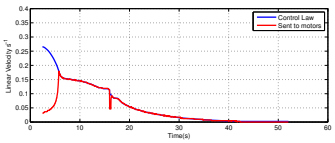

(a) Linear velocity command

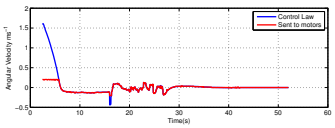

(b) Angular velocity command

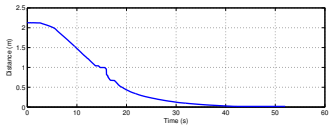

(c) e.

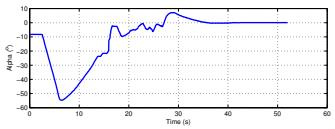

(d) α.

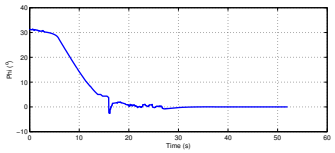

(e) ϕ.

Fig. 19: Time progression of state variables and commands.

VIII. Conclusions

A sensor-based positioning system based on measurements from optical encoders and from feature recognition using an RGB-D camera is proposed and experimentally validated. The proposed estimation system is able to localise a certain feature in the environment, tracking it even if it is not in sight, by estimating any slippage that might be occurring in the wheels for a better open-loop navigation. The Kalman filtering solution makes use of a new linear differential drive mobile robot kinematics by representing the movement of the environment in the robot frame instead of the inverse, allowing for a sub-optimal linear estimation and noise reduction due to the fact that no rotation is executed. The estimate is seen to converge rapidly once a landmark is in sight and also to be globally stable in faulty initializations or kidnapping scenarios. The slippage estimation contributes positively for the localisation in open-loop if the robot does not change its speed too drastically, seing as the slippage takes some time to be estimated due to the choice of values for $\mathbf{Q}$ and $\mathbf{R}$, which were chosen so as to smooth the estimate and also avoid the slippage estimate to respond to noise or faulty measurements.

The devised feedback control successfully drives the robot to a given goal and is tunable to the needs of the localisation system, seeing as it is possible to require the robot to take the same path under different speeds by just adjusting the parameters that tune the feedback. It is also possible to achieve good results by imposing a saturation in linear and angular velocities as to ensure convergence of the localisation system within the manoeuvre time frame. The robot is able to drive itself to the correct goal even when a wrong initial position and attitude estimate occurs, given that the landmark is visible. Also the localisation system is able to reject some of the corrupt camera measurements allowing for a smoother driving.

Notwithstanding the fact that the present thesis carried out its purpose, there is still, as always, room for improvement. Regarding the theoretical work, the localisation was devised to track a static landmark, giving the opportunity for future work to address the problem of localising a moving robot by also using a on-board vision based system. Also, now regarding the control law, the devised feedback law is easily extendable to the case where the goal is moving through the inertial frame by following in works in [3]. By also making use of Lyapunov techniques it is possible to add collision avoidance capabilities to the present system.

Acknowledgements

My thanks goes to Professor Miguel Tavares, for letting me visit the Biomechanics Laboratory of Lisbon and assisting me by collecting the experimental data that greatly contributed to the validation of this work.

This work was partially supported by : i) the project PRODUTECH-PTI (P. 3904) under the program COMPETE/QREN/FEDER; ii) FCT, through IDMEC, under LAETA; and iii) the project PTDC/EEA-CRO/102102/2008, IDMEC.

References

[1] Qualysis motion capture system. http://www.qualisys.com. Accessed: 2013-07-10.

[2] G. J. Agin. *Real time control of a robot with a mobile camera*. SRI International, 1979.

[3] M. Aicardi, G. Casalino, A. Bicchi, and A. Balestrino. Closed loop steering of unicycle like vehicles via lyapunov techniques. *Robotics & Automation Magazine, IEEE*, 2(1):27–35, 1995.

[4] P. Batista, C. Silvestre, and P. Oliveira. A two-step control strategy for docking of autonomous underwater vehicles. In *American Control Conference (ACC), 2012*, pages 5395–5400. IEEE, 2012.

[5] R. W. Brockett et al. Asymptotic stability and feedback stabilization. In *Differential Geometric Control Theory*, pages 181–191. Defense Technical Information Center, 1983.

[6] J. Chen, W. E. Dixon, M. Dawson, and M. McIntyre. Homography-based visual servo tracking control of a wheeled mobile robot. *Robotics, IEEE Transactions on*, 22(2):406–415, 2006.

[7] B. Espiau, F. Chaumette, and P. Rives. A new approach to visual servoing in robotics. *Robotics and Automation, IEEE Transactions on*, 8(3):313–326, 1992.

[8] M. D. Feezor, F. Yates Sorrell, P. R. Blankinship, and J. G. Bellingham. Autonomous underwater vehicle homing/docking via electromagnetic guidance. *Oceanic Engineering, IEEE Journal of*, 26(4):515–521, 2001.

[9] Y. Hada and S. Yuta. A first-stage experiment of long term activity of autonomous mobile robotâĂŤresult of repetitive base-docking over a week. In *Experimental Robotics VII*, pages 229–238. Springer, 2001.

[10] S. Hutchinson, G. D. Hager, and P. I. Corke. A tutorial on visual servo control. *Robotics and Automation, IEEE Transactions on*, 12(5):651–670, 1996.

[11] M. Kim and N. Y. Chong. Direction sensing rfid reader for mobile robot navigation. *Automation Science and Engineering, IEEE Transactions on*, 6(1):44–54, 2009.

[12] O. Lefebvre and F. Lamiraux. Docking task for nonholonomic mobile robots. In *Robotics and Automation, 2006. ICRA 2006. Proceedings 2006 IEEE International Conference on*, pages 3736–3741. IEEE, 2006.

[13] R. C. Luo, C. T. Liao, K. L. Su, and K. C. Lin. Automatic docking and recharging system for autonomous security robot. In *Intelligent Robots and Systems, 2005.(IROS 2005). 2005 IEEE/RSJ International Conference on*, pages 2953–2958. IEEE, 2005.

[14] C. McCarthy, N. Barnes, and R. Mahony. A robust docking strategy for a mobile robot using flow field divergence. *Robotics, IEEE Transactions on*, 24(4):832–842, 2008.

[15] J.-Y. Park, B.-H. Jun, P.-M. Lee, F.-Y. Lee, and J.-h. Oh. Experiment on underwater docking of an autonomous underwater vehicleisimi'using optical terminal guidance. In *OCEANS 2007-Europe*, pages 1–6. IEEE, 2007.

[16] C. Samson, B. Espiau, and M. L. Borgne. *Robot control: the task function approach*. Oxford University Press, 1991.

[17] S. B. Skaar, I. Yalda-Mooshabad, and W. H. Brockman. Nonholonomic camera-space manipulation. *Robotics and Automation, IEEE Transactions on*, 8(4):464–479, 1992.